A Study of Vibrational Relaxation of B-State Carbon Monoxide in the Heme Pocket of Photolyzed Carboxymyoglobin

Diane E. Sagnella and John E. Straub
Department of Chemistry, Boston University, Boston, Massachusetts 02215

ABSTRACT   The vibrational energy relaxation of dissociated carbon monoxide in the heme pocket of sperm whale myoglobin has been studied using equilibrium molecular dynamics simulation and normal mode analysis methods. Molecular dynamics trajectories of solvated myoglobin were run at 300 K for both the δ- and ϵ-tautomers of the distal histidine, His[64]. Vibrational population relaxation times were estimated using the Landau–Teller model. For carbon monoxide (CO) in the myoglobin ϵ-tautomer, for a frequency of $\omega_0 = 2131$ cm^{-1} corresponding to the B_1 state, $T_1^\epsilon(B_1) = 640 \pm 185$ ps, and for a frequency of $\omega_0 = 2119$ cm^{-1} corresponding to the B_2 state, $T_1^\epsilon(B_2) = 590 \pm 175$ ps. Although the CO relaxation rates in both the ϵ- and δ-tautomers are similar in magnitude, the simulations predict that the vibrational relaxation of the CO is faster in the δ-tautomer. For CO in the myoglobin δ-tautomer, it was found that the relaxation times were identical within error for the two CO substate frequencies, $T_1^\delta(B_1) = 335 \pm 115$ ps and $T_1^\delta(B_2) = 330 \pm 145$ ps. These simulation results are in reasonable agreement with experimental results of Anfinrud and coworkers (unpublished results). Normal mode calculations were used to identify the dominant coupling between the protein and CO molecules. The calculations suggest that the residues of the myoglobin pocket, acting as a first solvation shell to the CO molecule, contribute the primary "doorway" modes in the vibrational relaxation of the oscillator.

BACKGROUND

The flow of excess vibrational energy into or out of vibrational modes is important to many reactions in which there is bond breaking or formation. One such reaction is carbon monoxide (CO) dissociation and rebinding in heme proteins. Investigation of CO relaxation in heme proteins can provide vital information concerning the cooperative nature of ligand binding and rebinding, in particular, and protein dynamics, in general.

Vibrational relaxation processes of carbonyl compounds have received considerable attention with the advent of ultra-fast time resolved laser methods (King et al., 1993). The population relaxation times for metal carbonyls vary considerably from molecule to molecule, ranging from the picosecond to nanosecond timescales. This demonstrates that the local environment influences the vibrational relaxation time (T_1) of the carbonyl. To date, there have been several experimental probes into the vibrational relaxation of CO in model heme compounds (Hill et al., 1995) and heme proteins (Hill et al., 1994; Owrutsky et al., 1995). These studies have focused on the population relaxation of the bound CO, which, in the heme protein, myoglobin, is called the A-states.

The vibrational lifetime of bound CO in myoglobin is strongly dependent on the structure of the surrounding protein. Vibrational relaxation of bound CO in heme proteins is very fast compared to other CO-ligated compounds (Hill et al., 1995; Owrutsky et al., 1995). For example, Owrutsky et al. (1995) have found that the CO vibrational lifetime in heme proteins is ~20 ps, while King and coworkers (1993) have found a 150-ps time scale in the relaxation of the CO stretch in first row transition metal carbonyl compounds.

To justify the fast relaxation of bound CO in heme proteins, it has been suggested that the manifold of states within the heme are responsible (Hill et al., 1996a). Vibrational relaxation tends to be more efficient through strong covalent interactions, and this appears to be true in MbCO. Although there is only one such interaction between the CO and the heme, studies indicate that intermolecular transfer of vibrational energy is relatively unimportant in the relaxation process of bound CO (Hill et al., 1996a).

Interestingly, vibrational lifetimes also differ within the same protein but in different conformational substates (Hill et al., 1994). Hill and coworkers (1996b) have shown that changes in the vibrational lifetime of bound CO are correlated with changes in the frequency of the CO molecule that accompany such transitions. Moreover, Fayer and coworkers have found that the T_1 population relaxation time for the carbonyl ligand is only slightly dependent on temperature, decreasing ~10% from 50 to 300 K. They concluded that the low frequency bath modes do not play a significant role in the relaxation of bound CO (Hill et al., 1994).

In contrast to this detailed understanding of CO energy relaxation in metal carbonyls and the bound A-states of carboxy myoglobin, little is known about the relaxation time scale or mechanism in the photolyzed state. After dissociation of the CO from the heme at room temperature, the CO quickly finds itself in one of two B-states. These states are identified by a change in the CO vibrational frequency from ~1960 to ~2131 cm^{-1} or ~2119 cm^{-1} for B_1 and B_2, respectively. Anfinrud and coworkers have investigated the B-states and contend that the CO is in one of

two orientations within a binding site located in the heme pocket (Lim et al., 1995).

The CO in the B-state has no covalent interactions. Any contribution of the heme or protein to its relaxation may give a picture of the role of the protein solvent in the relaxation of the CO in the bound and photolyzed states. This paper describes a computational study of the CO population relaxation and mechanism of the photolyzed state using molecular dynamics and normal mode analysis of the fully solvated, room-temperature myoglobin system.

Calculation of the vibrational relaxation time (T_1)

The process of vibrational relaxation involves the dissipation of excess vibrational energy into the surroundings. Zwanzig (1973) showed that, when a system can be represented by the generalized Langevin equation, the time decay of the vibrational energy relaxation is a single exponential (the Landau–Teller result)

$$\frac{\langle E_v(t)\rangle - \langle E_v(\infty)\rangle}{\langle E_v(0)\rangle - \langle E_v(\infty)\rangle} = \exp(-t/T_1), \qquad (1)$$

where the brackets $\langle \cdots \rangle$ indicate an average over initial zero time states. Using this formalism along with the assumption that the oscillator is anharmonic and is linearly coupled to the solvent, an expression for T_1 (Oxtoby, 1979; Oxtoby, 1981; Zwanzig, 1961) can be obtained

$$\frac{1}{T_1} = \frac{1}{\mu} \int_0^\infty dt \, \cos(\omega_0 t)\zeta(t), \qquad (2)$$

where μ is the reduced mass

$$\mu = \frac{m_c m_o}{m_c + m_o}, \qquad (3)$$

and ω_0 is the frequency of the oscillator. The time dependent friction, $\zeta(t)$, is a measure of the dissipation force along the oscillator's vibrational coordinate.

Time correlation functions of harmonic quantum systems can be directly related to those of the corresponding classical systems. Bader and Berne (1994) have shown this result in the context of vibrational relaxation that, if the system can be described by a set of harmonic normal modes, the relaxation time obtained in a fully quantum system (quantum solute in a quantum bath) is the same as that obtained from a fully classical simulation (classical solute in a classical bath). Furthermore, they suggest that this result may also be applicable when anharmonicities are present. Therefore, it is conceivable that accurate values for vibrational population relaxation times in myoglobin can be obtained from classical molecular dynamics simulations, provided the bath and system–bath coupling are well described as harmonic.

The time-dependent friction is proportional to the time correlation function of the fluctuating random force on the bond. When the bond is of high frequency, it can be considered rigid, and molecular dynamics are run with the oscillator (CO molecule) constrained at its equilibrium distance (Berne et al., 1990). The friction kernel in Eq. 2 can then be easily computed in the rigid bond approximation where $\zeta(t)$ can be written,

$$\zeta(t) = \frac{1}{k_b T}\langle \delta F(t)\delta F(0)\rangle. \qquad (4)$$

$\delta F(t) = F(t) - \bar{F}$ is the fluctuating solvent force on the oscillator bond. The force correlation function includes the effects of the density of states and coupling strength of the surrounding solvent. The scalar force along the bond is determined using

$$F = \mu\left(\frac{\mathbf{F}_c}{m_c} - \frac{\mathbf{F}_o}{m_o}\right)\cdot \hat{\mathbf{r}}_{co}, \qquad (5)$$

where $\mathbf{F}_i$ is the force felt by atom i of the CO molecule due to the solvent, and $\hat{\mathbf{r}}_{co}$ is the CO bond unit vector.

In the case of CO, the assumptions made above are not unreasonable. CO is ground-state dominated, and the bottom of its bond potential can be accurately modeled as harmonic. Furthermore, in myoglobin, the coupling between the protein and the free CO is believed to be weak. Finally, the CO bond is a high frequency oscillator ($\omega_0 \sim 2140$ cm^{-1}), for which the rigid bond approximation holds. (This limit has also been found to be reasonable for low frequency oscillators, an indication of the robustness of the approximation (Berne et al., 1990).) The applicability of equilibrium molecular dynamics in the study of relaxation processes is supported by work done by Whitnell (1990, 1992), in which both equilibrium and nonequilibrium techniques were used to determine vibrational relaxation times. With each method, a similar value for T_1 was found, suggesting that the vibrational relaxation is adequately described by the linear response approximation.

Normal mode analysis

To examine the mechanism of energy relaxation, it is essential to be able to identify those protein modes that are most strongly coupled to the CO bond stretching mode. This can be accomplished by a normal mode analysis based on quenched normal modes (QNM) or instantaneous normal modes (INM). The set of QNM is computed by a diagonalization of the Hessian matrix for a set of equilibrium configurations minimized prior to diagonalization. The QNM method offers a straightforward way to separate and examine the coupling between the system and bath modes.

A good deal of attention has been given to the use of INM in the determination of short time dynamical properties of simple solutes in liquids (Cho et al., 1994; Goodyear and Stratt, 1996, 1997; Ladanyi and Stratt 1998). The INM method involves diagonalizing the Hessian matrix for a set of instantaneous configurations taken from a dynamical trajectory (Seeley and Keyes, 1989). Because these config-

urations are not necessarily at the potential minimum, there are both real frequencies corresponding to stable oscillations of the system and imaginary frequencies corresponding to unstable motion of the system. These imaginary modes tend not to couple strongly to solute molecules (Wann and Stratt, 1994). (As a result, the imaginary modes were excluded in the calculation of the friction kernel presented in this work.) The INM formalism can be used to describe short-time dynamics. In fact, if the time increment δt is infinitesimally small, the INM method is exact. The INM method can also be used to calculate the fluctuating friction along a bond as shown by Goodyear and Stratt (1996, 1997). When using a normal mode model to calculate the friction along a vibrational coordinate, we begin with Zwanzig's model of an anharmonic system oscillator r, bilinearly coupled to a bath of harmonic oscillators x_i. In other words,

$$H = H_{osc}(p, r) + \sum_i \left(\frac{1}{2m_i} P_i^2 + \frac{1}{2} m_i \omega_i^2 x_i^2 + c_i x_i r \right), \quad (6)$$

where

$$H_{osc}(p, r) = \frac{1}{2\mu} p^2 + V_{osc}(r). \quad (7)$$

Changing to mass-weighted coordinates, the Hamiltonian becomes

$$H = H_{osc}(\bar{p}, \bar{r}) + \sum_i \left(\frac{1}{2} \bar{P}_i^2 + \frac{1}{2} \omega_i^2 \bar{x}_i^2 + C_i \bar{x}_i \bar{r} \right). \quad (8)$$

Zwanzig derived the time-dependent friction from the Hamiltonian (Eq. 8) and found

$$\zeta(t) = \sum_i \left(\frac{C_i}{\omega_i} \right)^2 \cos(\omega_i t) = \beta \langle \delta F(t) \delta F(0) \rangle. \quad (9)$$

The sum in Eq. 9 is over the normal modes of the bath oscillators i with mode frequency ω_i. The key to Eq. 9 is the coupling constants, C_i, between the bath coordinates and the oscillator (CO) stretching coordinate. When considering vibrational relaxation, the couplings should be a measure of how the bath modes affect the force along the CO bond,

$$C_i = \frac{\partial F}{\partial q_i}, \quad (10)$$

where q_i are the mass-weighted normal mode coordinates. The force along the CO bond is

$$F = -\frac{dV}{dr_{CO}} = -\mu \left(\frac{1}{m_c} \frac{\partial V}{\partial \mathbf{r}_c} - \frac{1}{m_o} \frac{\partial V}{\partial \mathbf{r}_o} \right) \cdot \hat{\mathbf{r}}_{CO}, \quad (11)$$

where V is the interaction potential between the carbon monoxide molecule and the surroundings. The expression for the coupling constants can then be written with respect to the mass-weighted Hessian matrix used in the determi-

nation of the normal modes

$$C_i = -\sum_j^N \frac{1}{\sqrt{m_j}} \frac{\partial^2 V}{\partial x_j \partial r_{co}} \frac{\partial x_j}{\partial q_i} \quad (12)$$

$$= -\sum_j^N \frac{C_j^*}{\sqrt{m_j}} \frac{\partial x_j}{\partial q_i}. \quad (13)$$

The $\partial x_j / \partial q_i$ terms are the coefficients of the eigenvector matrix of the normal modes, which will be denoted as $U_{i,j}$.

Normal mode calculations can also be used to examine the role of collective motions in the dynamics of the system. We compute the participation ratios defined as

$$R_i^I = \sum_j^{3N} (U_{i,j})^4 \quad (14)$$

and

$$R_i^{II} = \sum_l^{M \text{ residues}} \left[\sum_j^{3N_l} U_{i,j}^2 \right]^2. \quad (15)$$

The sum in Eq. 14 is over all $3N$ degrees of freedom in the system. In Eq. 15, the summation is divided into two components. The sum over l extends over the M residues in the NM calculation; the second sum over j extends over the $3N_l$ degrees of freedom of residue l.

The inverses of R_i^I and R_i^{II} are a measure of the degree of localization of each mode. $1/R_i^I$ corresponds to the number of atoms participating in the ith mode, while $1/R_i^{II}$ corresponds to the number of residues and water molecules participating in the ith mode. If mode i is completely delocalized, $1/R_i^I$ should be a good estimate of the number of degrees of freedom of the system, $3N$, and $1/R_i^{II}$ should be a good estimate of the number of residues and water molecules that contribute to that mode. If a mode is completely localized so that only one local mode participates in the mode, only one of the eigenvector coefficients would be nonzero. Because the eigenvectors are normalized, that coefficient and $1/R_i^I$ would be equal to unity. Conversely, if the mode is fully delocalized, each degree of freedom would be equally involved. Therefore,

$$U_{i,j}^2 = \frac{1}{3N} \quad (16)$$

and

$$R_i^I = \sum_j^{3N} \left(\frac{1}{3N} \right)^2 = \frac{1}{3N}. \quad (17)$$

In this work, the classical equilibrium molecular dynamics method is used to calculate the T_1 time of CO in the heme pocket of myoglobin. Second, using normal mode techniques, the coupling of the protein-solvent environment to the CO oscillator has been investigated. From these

couplings, a friction kernel has been calculated and compared with the molecular dynamics results. The coupling constants have been used to identify bath modes important to the mechanism of CO vibrational relaxation in myoglobin.

COMPUTATIONAL MODEL AND METHODS

The sperm whale myoglobin molecule (Schlichting et al., 1994) was placed in a $56.70 \times 56.70 \times 37.712$ Å^3 box and simulated using periodic boundary conditions. A previously equilibrated box of TIP3P water molecules (Jorgensen et al., 1983) was overlayed and any water molecule whose oxygen atom was within 2.5 Å of a nonhydrogen protein atom was removed. The all-hydrogen parameter set (version 25) within CHARMM (MacKerell et al., 1992) was used. The system, in its entirety, was composed of 11,499 atoms; 2551 myoglobin atoms, 2982 water molecules, and the two atoms of CO. To minimize any bad contacts or unusual strain, ~1500 steepest descent energy minimization were performed.

Molecular dynamics

The temperature was increased slowly to 300 K using the following protocol. From 0 to 150 K, the temperature was increased 10% after every 2-ps of molecular dynamics by randomly sampling the atomic velocities from a Maxwell distribution. The criteria for velocity resampling was based on a 5% temperature window. From 150 to 215 K, the temperature was scaled by 5% and the window became 2.5% of the current temperature. When the temperature reached 215 K, the temperature window became constant at 5 K with an interval of 4 ps between velocity resamplings.

After a temperature of 300 K was reached, 20 ps of constant temperature molecular dynamics was run, in which the temperature was checked every 10 fs. During the last 10 ps, the average temperature remained within the 5 K window and there was no need to resample the atomic velocities. At this point, it was assumed that an equilibrium state had been reached and data could be collected from constant energy dynamics. Microcanonical trajectories of varying lengths (10–20 ps) were run for a total of 350 ps for the ϵ-tautomer and 200 ps for δ-tautomer. The entire 350 ps of the ϵ trajectories were used in determining the T_1 times; however, only 150 ps were used in the decomposition of the force autocorrelation function and its comparison with the δ-tautomer. The molecular dynamics timestep was 1.0 fs and the intermolecular potential was truncated at 10.5 Å using a group switching function from 9.5 Å.

The three-site model of Straub and Karplus (Ma et al., 1997; Straub and Karplus, 1991), in which charges are placed on the carbon and oxygen atoms as well as the center of mass, was used to represent the CO. This simple charge model, when combined with the Huffaker RRKR potential for the bond (Huffaker, 1976), has been shown to reproduce the experimental dipole and quadrupole moments of the CO molecule, as well as ab initio interaction energies of CO with a variety of molecules, including water and formamide. Interactions between the CO molecule and the protein-solvent environment involve a Lennard–Jones contribution and a three-site electrostatic term,

$$V = \sum_j \left[\sum_{i=1}^3 \frac{Q_i Q_j}{r_{ij}} + \sum_{i=1,2} 4\epsilon_{ij} \left(\left(\frac{\sigma_{ij}}{r_{ij}} \right)^{12} - \left(\frac{\sigma_{ij}}{r_{ij}} \right)^6 \right) \right], \quad (18)$$

where Q_i is the charge on site i and r_{ij} is the distance between sites i and j. The Lennard–Jones parameters, σ_{ij} and ϵ_{ij}, are determined via (Lorentz–Berthelot combining rules)

$$\sigma_{ij} = \frac{\sigma_i + \sigma_j}{2} \qquad \epsilon_{ij} = \sqrt{\epsilon_i \epsilon_j}. \quad (19)$$

The first term in Eq. 18 describes the Coulombic interactions in which the second summation is over the three sites of the CO molecule (the carbon

and oxygen atoms and the center of mass). The second term is the van der Waals contribution in which the summations involve interactions between the carbon and oxygen atoms of the CO molecule and the surrounding protein and solvent atoms.

The CO bond was constrained to its equilibrium position (1.128 Å) using the SHAKE algorithm. The fluctuating force autocorrelation function was calculated, and its Fourier transform was carried out using fast Fourier transform (FFT) techniques (Press et al., 1989).

Normal modes

The density of states of a given system can provide insight into possible modes available for vibrational relaxation of the CO molecule, and is given by

$$D(\omega) = \frac{1}{3N} \left\langle \sum_i^N \delta[\omega - \omega_i] \right\rangle. \quad (20)$$

To identify relaxation pathways for the CO molecule in the myoglobin pocket, several quenched and instantaneous normal mode calculations were performed on subsets of the solvated myoglobin system. Several configurations were picked from equilibrium trajectories. For each of these configurations, any residue whose center of mass was outside a 14.0-Å radius from the center of mass of the CO molecule was removed. For the QNM calculations, this system subset was then minimized using the adopted basis Newton–Raphson (ABNR) method (Brooks et al., 1983). To help maintain the system integrity in the vicinity of the CO molecule, a harmonic restoring force was applied to all atoms beyond a 12.0-Å radius from the CO molecule. The above distances were chosen after several tests indicating that a 14.0-Å cutoff was sufficient to achieve converged minimized geometries near the CO as well as the density of states. The reduced system was used to reduce the associated computational overhead. The harmonic restoring force constant was set at 1.0 kcal/(mol Å^2). The INM calculations were performed on the system subset without additional constraints. The system subset was diagonalized without potential energy truncation or periodic boundary conditions.

RESULTS

In this section, values of T_1 are estimated, normal mode methods are used to determine important doorway modes in the protein and solvent, and the dominant contributors to the relaxation process are identified.

CO population relaxation times

As described above, relaxation times of high frequency oscillators can be directly related to the Fourier transform of the fluctuating force–force autocorrelation function $\langle \delta F(0) \delta F(t) \rangle$ of the force along a rigid bond. In determining the vibrational relaxation time, the value of the friction kernel at the frequency of the oscillator is used. The friction kernel $\breve{\zeta}(\omega)$ as a function of frequency calculated from the above simulations for the ϵ and δ-tautomers is shown in Fig. 1. The arrow points to the frequency of the free CO bond and the inlay depicts the time dependence of $\langle \delta F(0) \delta F(t) \rangle$. Using this method and

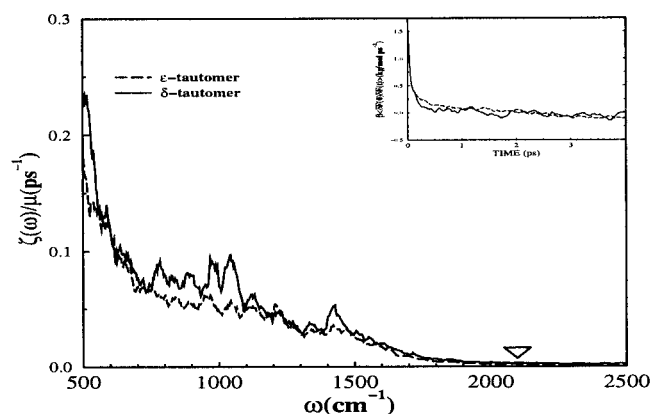$$\frac{1}{T_1} = \frac{\zeta(\omega_0)}{\mu}, \quad (21)$$

FIGURE 1   The frequency-dependent friction kernels, $\zeta(\omega)$, for the carbon monoxide ligand in the heme pocket of sperm whale myoglobin (ϵ and δ-tautomers) are shown. Displayed in the inlay is the fluctuating force autocorrelation function for the carbon monoxide ligand stretch. These functions were averaged over 350 (ϵ) and 175 (δ) ps of CO dynamics in the heme pocket at 300 K. The $\triangledown$ marks the CO oscillator frequency at 2100 cm^{-1}. The $\zeta(\omega)$ data have been smoothed for clarity.

the relaxation time of the CO oscillator was estimated.

The spectrum of the time-dependent friction was somewhat noisy. To remove some of the noise, the spectra were smoothed by locally averaging over the data points. This provided an average value, $\bar{\zeta}$, at the frequency of the oscillator, as well as a standard deviation, σ_ζ, for each point. We related the standard deviation to the uncertainty in our estimate of the relaxation time as

$$\sigma_{T_1} = \mu \frac{\sigma_\zeta}{\bar{\zeta}^2}. \qquad (22)$$

Table 1 lists the values obtained by averaging over 2, 5, and 10 points. As can be seen, the values obtained are all within the calculated error of each other. We chose to use a value of 10 for averaging over all spectra presented in this work.

In Table 1, we present several vibrational relaxation times for the various B-states. Because interconversion between B_1 and B_2 is a spontaneous process at 300 K, the force along the CO molecule calculated is probably due to both B_1 and

TABLE 1   CO vibrational relaxation times computed for the ϵ and δ tautomers of sperm whale myoglobin

		T_1			σ		
	ω	2	5	10	2	5	10
ϵ	2119	615	600	590	215	190	175
	2131	790	630	640	195	160	185
δ	2119	435	355	330	105	90	115
	2131	295	320	335	135	120	145

The calculation of the T_1 times were done by locally averaging over the FFT spectrum of the force autocorrelation function. This was done over 2, 5, and 10 points as indicated in the table, showing the relative insensitivity of the results to the method chosen. The frequency ω is in units of cm^{-1} and T_1 and σ are in ps. The values reported in the present paper are those obtained by locally averaging over 10 points.

B_2 substates. Therefore, care should be taken not to attribute too much significance to the differences in the T_1 times for the different substates. The results reported are an average over the substates and should be viewed as such. Nonetheless, these values for the vibrational relaxation time are in very good agreement with the experimental value of ~600 ps determined by Anfinrud (submitted for publication). It is interesting to note that the T_1 time calculated for the ϵ-tautomer is in closer agreement with the experimental result than that for the δ-tautomer. Because the time scale for tautomerization is much longer than that for the photolyzed CO to enter the B-states, our results suggest that the ϵ-tautomer may be present at the time of photolysis. Although this interpretation contradicts the neutron crystal data of Schoenborn (Hanson and Schoenborn, 1981; Cheng and Schoenborn, 1991), recent resonance Raman work indicates the presence of the H_ϵ in carbonmonoxy myoglobin (Unno et al., 1998).

The use of Eq. 2 and the equilibrium molecular dynamics methods illustrated in this paper have proven to be an effective method in determining population relaxation times for a number of other systems (Gnanakaran and Hochstrasser, 1996; Whitnell et al., 1992), demonstrating the wide applicability of the method and supporting our use of the Landau–Teller approach.

From the data in Table 1, it appears that the T_1 time of the B-state CO population relaxation is considerably slower than the ~17 ps found for CO in its bound state. (Owrutsky et al., 1995). This suggests that the Fe–CO bond and the heme itself contribute to A-state CO relaxation. This comes as no surprise. Owrutsky and co-workers (1995) and Hill et al. (1996a, b) have suggested that π-backbonding plays a role in the relaxation process. In studies of vibrational relaxation of model heme compounds, Fayer and coworkers (Hill et al., 1996a, b) go further in saying that anharmonic coupling through the π bond provides the dominant pathway of relaxation.

Normal mode calculations

The density of states determined using the QNM and INM formalisms is shown in Fig. 2. The direct contribution of the restraining force used in the QNM calculation has been removed. The resulting peak appears at ~155 cm^{-1} and does not change any of the observations mentioned. As expected, the INM spectrum possesses imaginary modes, plotted here in the standard way along the negative frequency axis. These imaginary frequencies make up approximately 5% of $D(\omega)$. Although Lennard–Jones fluids exhibit much higher relative numbers of imaginary modes (Wan and Stratt, 1994; Wu and Loring, 1992; Madan et al., 1990; Madan and Keyes, 1993; Seeley et al., 1991), the result presented here is similar in magnitude to results seen in crystals or ordered liquids such as liquid water (Cho et al., 1994). The most noticeable difference between the two methods is an apparent smearing of states in our INM
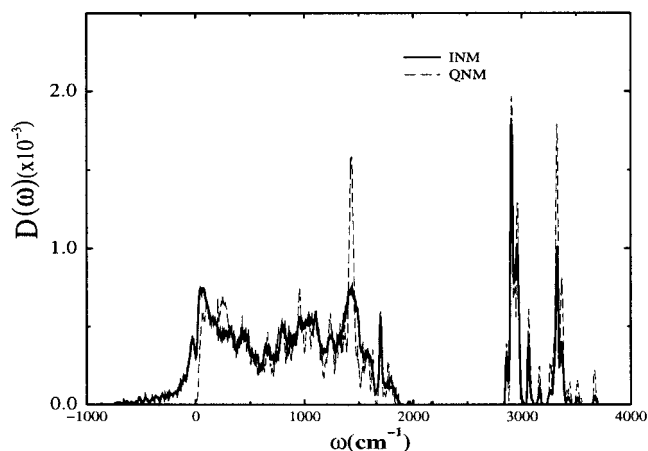
FIGURE 2   The density of states as defined by Eq. 20 from QNM and INM calculations. The data have been smoothed for clarity and normalized so that they have unit area.

calculation. This behavior is due in part to the thermal energy of the atoms, a feature lacking in the QNM calculation. Perhaps more importantly, the spreading of states seen in Fig. 2 is an indication of the increasing importance of anharmonicities as trajectories move up the potential energy surface. This is especially evident at lower frequen-cies, in particular, from 1200 to 1600 cm^{-1}. In both spectra, there is a clear separation of states between 2000 and 2800 cm^{-1}. This separation effectively isolates the CO vibration from the remainder of the system, as a result CO vibrational coupling to the system is weak.

Figure 3 a and b, displays the inverse participation ratios for the INM calculations. The low frequency modes are quite delocalized with the lowest frequency modes corre-sponding to translational and rotational motion. With in-creasing frequency, the modes become more localized. Modes from 2000 to 3200 cm^{-1} involve only 1–2 residues. At higher frequencies, we see a decrease in localization due to the numerous OH and NH stretching modes. Nonetheless, the overall degree of localization remains considerable.

The distribution of the square of the coupling constants found in Eq. 10, also called the influence spectrum, is shown in Fig. 4 for the ϵ-tautomer. The most noticeable peak is at a frequency of ~3515 cm^{-1} corresponding to the N_ϵ-H_ϵ stretch of the distal histidine, His^{64}. The second most prominent peak can be seen in the region of 1500–1700 cm^{-1}. The modes found here are a combination of angle bending and bond stretching motions with His^{64} playing a key role. The influence spectrum for the δ-tautomer exhib-ited similar couplings to the vibrational modes of the distal histidine (with the exception of the absent N_ϵ-H_ϵ stretch).
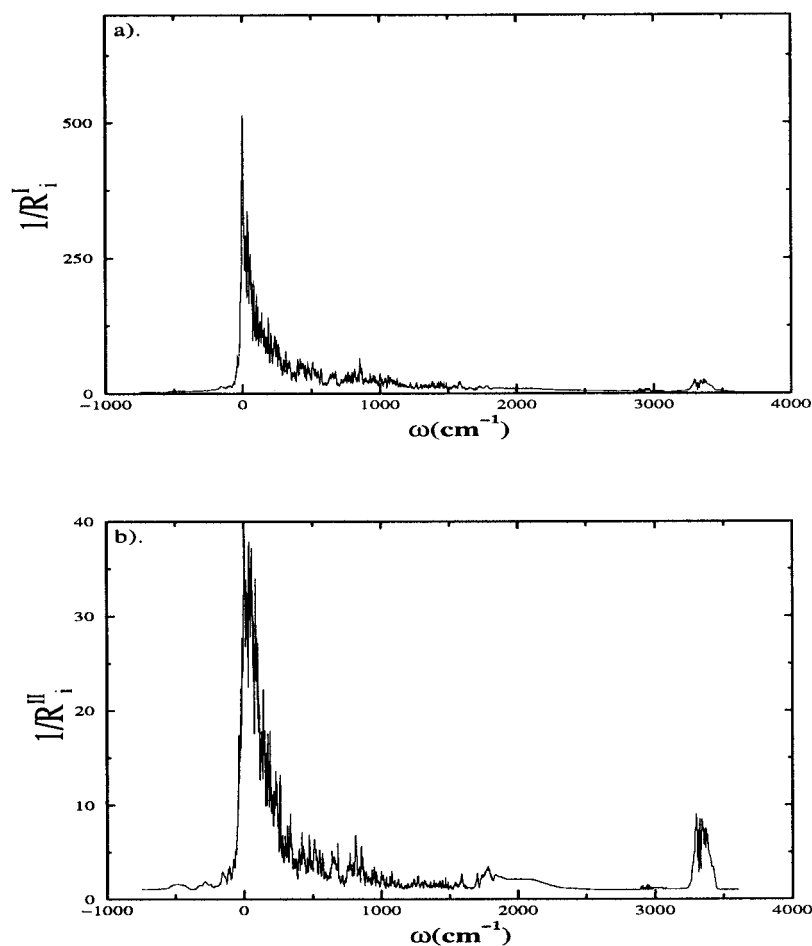
FIGURE 3   The inverse participation ratios as deter-mined from the eigenvectors of the QNM and INM calculations described in the text. (a) The number of degrees of freedom involved in a given mode. (b) The number of residues or water molecules involved in a given mode. The data have been smoothed for clarity.
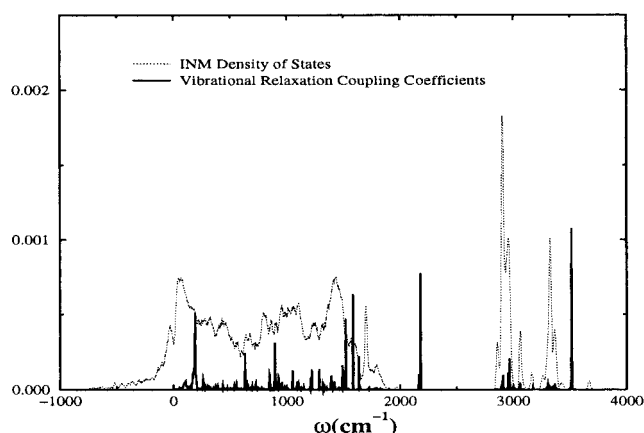
FIGURE 4 The square of the vibrational coupling constants against a backdrop of the INM density of states for myoglobin at 300 K. The results above are averaged over ten configurations taken from separate molecular dynamics trajectories. The spike at ~2100 cm^{-1} corresponds to the CO vibrational frequency.

TABLE 2 A list of residues believed to be key in the vibrational relaxation of free carbon monoxide in myoglobin

Residue	R (Å)	Frequency (cm^{-1})	Motion
Leu[29]	6.04	1325	Collective bond and angle motions with Leu[61]
		2960	C_γ-H_γ stretch
Phe[43]	7.43	3060	C_ζ-H_ζ, C_ϵ-H_ϵ
Leu[61]	8.24	1325	Collective bond and angle motions with Leu[29]
		2890	$C_{\delta 1}$-$H_{\delta 1}$ stretch
		2972	C-H stretches (70%)
His[64]	5.55	3515	N_ϵ-H_ϵ stretch
		1520	Ring stretching and bending
		1590	Ring stretching and bending
Val[68]	6.27	2955	Carbon-Hydrogen Stretch
		2990	C_γ-H_γ stretch
Heme	4.70	1090	Large collective heme motions
		1200	Large collective heme motions

Listed are the residue names, the distance between the center of mass of the residue and the CO molecule, the frequency at which strongest coupling is observed, and the motions corresponding to that frequency.

Although some solvent coupling is evident between 3200 and 3300 cm^{-1}, the effect appears to be minimal. This information, combined with that from the participation ratios shown in Fig. 3 *a* and *b*, suggest that the principle modes responsible for CO relaxation in myoglobin are highly localized. Large scale collective motions are relatively unimportant in the relaxation process. This is in agreement with the interpretation of experiments done by Hill et al. (1996a), in which they attributed high frequency, localized modes to the relaxation of the CO ligand in myoglobin. Furthermore, the residues most strongly involved in the relaxation tend to be those closest to the CO molecule. Hard collisions are most efficient and this is done via high frequency localized modes near the CO. This behavior is similar to that found in liquids, in which the fluctuations in the first solvation shell of an oscillator were found to contribute most strongly to vibrational relaxation.

Given that the protein environment is not a liquid, there is no first solvation shell per se. The surrounding protein is more like a flexible cage. The closest residues act as the first solvation shell, and their flexibility enhances the relaxation process. Table 2 lists the residues most strongly coupled to the CO. From Table 2, the role of side chain flexibility is evident. For example, the heme is the closest residue to the CO, however, its coupling to the CO bond is small. This is due to the more or less rigid nature of the heme, which lacks the necessary flexibility for relaxation of the free CO. Interestingly, the coupling of the heme evident near 1090 cm^{-1} involves a collective of bond stretches, angle bends, torsions, and improper torsions of the heme.

Using the INM approach, we have calculated a friction kernel for our system. It is pictured in Fig. 5 and compared with the direct result from the MD simulation. It should be stressed that the INM calculations were performed for 10 configurations and may not be converged. The density of states for the different configurations showed little variation

from one to another. However, the influence spectra and fluctuating force autocorrelation functions varied considerably. This is in agreement with the work of Goodyear and Stratt (1996), who have demonstrated how dramatically INM friction spectra can differ from configuration to configuration. The oscillations in the INM function and its zero time value are a result of the lack of convergence.

The INM method was used in hopes of gaining qualitative insight behind the relaxation and not for the purpose of assigning definitive values relating to it. Considering the underlying approximations, it is impressive that the INM friction kernel approximates the time dependence of the full MD trajectory average so well. For example, there are clearly two time scales involved in the relaxation. The first is a result of nearest neighbor collisions and the second is derived from longer range collective motion. Furthermore,
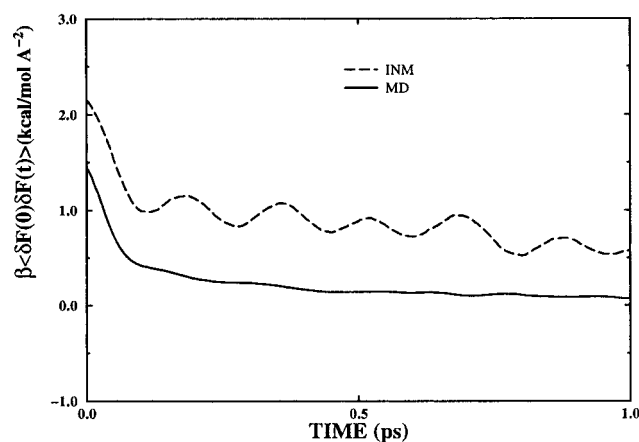

FIGURE 5 The friction kernels from the INM and molecular dynamics calculations at 300 K for the ε-tautomer.

the zero time value, although not correct, is of the right order of magnitude.

Testing the assumption of a harmonic bath

The molecular dynamics results presented here are encouraging in that they agree quite well with experimental measurement. A simple test to probe the validity of the harmonic approximation in treating the bath is given by the distribution of the fluctuating force along the bond. If the harmonic approach is appropriate, this distribution should be Gaussian. The result of this test can be seen in Fig. 6, in which a Gaussian fit to the data has been overlayed. As can be seen, the data, although not strictly Gaussian, do exhibit some Gaussian character and are reasonably approximated by a Gaussian distribution shifted to the left by 0.6 kcal/(mol Å). This is consistent with the good agreement between the Landau–Teller estimate for T_1 and the experimental result.

The 0.6 kcal/(mol Å) shift in Fig. 6 indicates an imbalance between forces that compress the bond and those that act to extend it. Which forces act to stretch the bond and which act to compress it? If the force along the bond is less than zero, the contributing force acts to expand the bond. Conversely, if the force along the bond is greater than zero, the effect is one of compression. Table 3 lists the force along the CO bond for the ϵ- and δ-tautomers. From this data, it is clear that the Coulombic force tends to stretch the CO bond whereas the LJ force tends to compress it.

The decomposition of the fluctuating force autocorrelation function

Further insight into the relaxation mechanism of the CO molecule in myoglobin can be gained via the decomposition of the fluctuating force autocorrelation function. Assuming
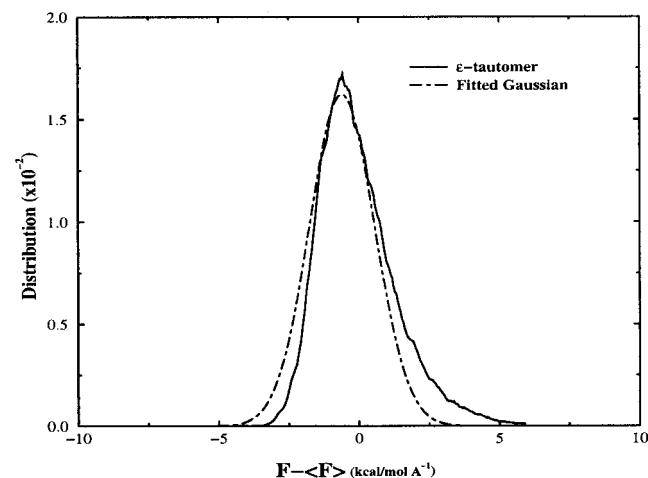

FIGURE 6   Comparison of fluctuating force distribution of the ϵ-tautomer with a Gaussian. The Gaussian fit was performed about the center of the original distribution and not about zero.

TABLE 3   The average Coulombic and Lennard–Jones forces felt along the CO vibrational coordinate for both the ϵ- and δ-tautomers of His[64] in myoglobin at 300 K

	Coulombic	Lennard–Jones
δ	−1.06	1.48
ϵ	−0.66	1.33

Units are in kcal/(mol Å).

that the potential can be expressed as pairwise interactions, the friction kernel may be decomposed into Lennard–Jones and Coulombic contributions as

$$\langle \delta F(0)\delta F(t)\rangle = \langle \delta F_{LJ}(0)\delta F_{LJ}(t)\rangle + \langle \delta F_{QQ}(0)\delta F_{QQ}(t)\rangle$$
$$+ \langle \delta F_{LJ}(0)\delta F_{QQ}(t)\rangle + \langle \delta F_{QQ}(0)\delta F_{LJ}(t)\rangle, \quad (23)$$

where F_{QQ} and F_{LJ} represent the Coulombic and Lennard–Jones contributions to the force. This should be possible due to the long range, long time scale Coulombic interactions and the short range, short time scale changes in the Lennard–Jones interactions. A similar decomposition may be accomplished by residue or entire segments of the system. For example, we can write

$$\langle \delta F(0)\delta F(t)\rangle = \langle \delta F_{prot}(0)\delta F_{prot}(t)\rangle + \langle \delta F_{heme}(0)\delta F_{heme}(t)\rangle$$
$$+ \langle \delta F_{solv}(0)\delta F_{solv}(t)\rangle + crossterms$$

where F_{prot}, F_{heme}, and F_{solv} indicate the force felt along the CO bond due to the protein, the heme and the solvent respectively.

The independent binary collision model (IBC) (Litovitz, 1957) has been used with success to describe vibrational relaxation in solution. This simple model views the events contributing to vibrational relaxation as separate independent collisions. Although there are criticisms of the model (Harris et al., 1990), it is proven to be useful in systems in which many bodied or long range interactions are minimal. This is not always the case in a protein bath. However, the CO molecule is relatively nonpolar molecule in a relatively nonpolar pocket. It may be that the IBC model is appropriate for this system in which the solvent is a protein. A more detailed decomposition by residue allows us to test the IBC model in which it is assumed that the effect of the cross terms is negligible. Although cross terms may contribute significantly to the friction, this may not be the case in the frequency domain. Therefore, the IBC model should be tested after the transform has been done and not before. In short, the IBC model assumes that

$$\zeta(\omega) \approx \sum_i \tilde{\zeta}_i(\omega), \quad (24)$$

where the sum over i is over the residues of the system and $\tilde{\zeta}(\omega)$ is the Fourier transform of the friction kernel $\zeta(t)$. Such an analysis can also give clues as to the relative importance

of specific regions of the protein in accepting excess vibrational energy from the CO molecule.

The fluctuating force distribution for the ϵ- and δ-tautomers is given in Fig. 7. Somewhat surprisingly, the distributions of the two tautomers are almost identical in height, width, and shift. Yet the distributions of the Coulombic and van der Waals components for the two tautomers differ. For example, the ϵ-tautomer's electrostatic force distribution is broader than the corresponding δ-tautomer's distribution. Therefore, although the magnitude of the average electrostatic force along the CO bond is greater for the δ-tautomer (as seen in Table 3), the fluctuations about this average are smaller. As a result the zero-frequency contribution to the friction kernel should be larger for the ϵ-tautomer (Gnanakaran and Hochstrasser, 1996). The Lennard–Jones force distributions of the two tautomers are fairly similar. They differ slightly in shift and height but are roughly equivalent in their widths. The long tail of the force distributions seen in Fig. 7 is due to close-range repulsive interactions felt by the CO molecule in the myoglobin pocket. Interestingly, the differences between the Coulombic and van der Waals distributions in the two tautomers balance each other so that the overall distributions are identical.

Although the vibrational relaxation of CO in myoglobin is due to fluctuations in both the electrostatic and Lennard–Jones forces, the major contribution is from relatively weak Lennard–Jones forces. This is demonstrated in Fig. 8 a and b, where the electrostatic and Lennard–Jones contributions to the friction spectrum for the two tautomers are presented. Clearly, the major contribution is due to the van der Waals interactions. This is not necessarily surprising. The CO molecule has a very small permanent dipole moment and moderate permanent quadrupole moment. However, it is likely that the electrostatic effects play a much larger role in the process of pure dephasing.

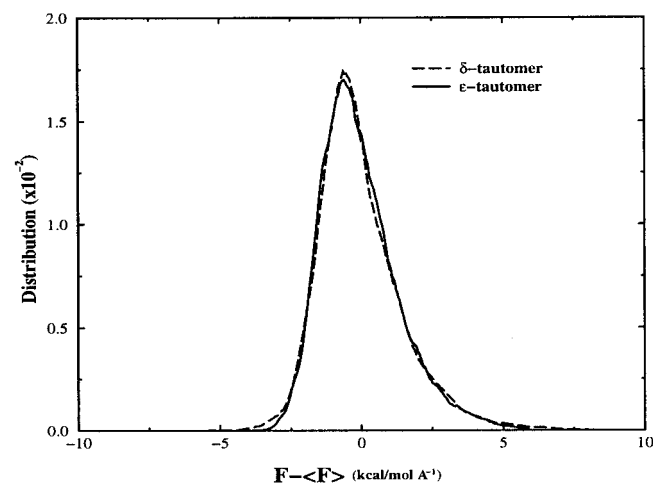To learn more about the vibrational mechanism of CO in the myoglobin pocket, several decompositions of the fluc-
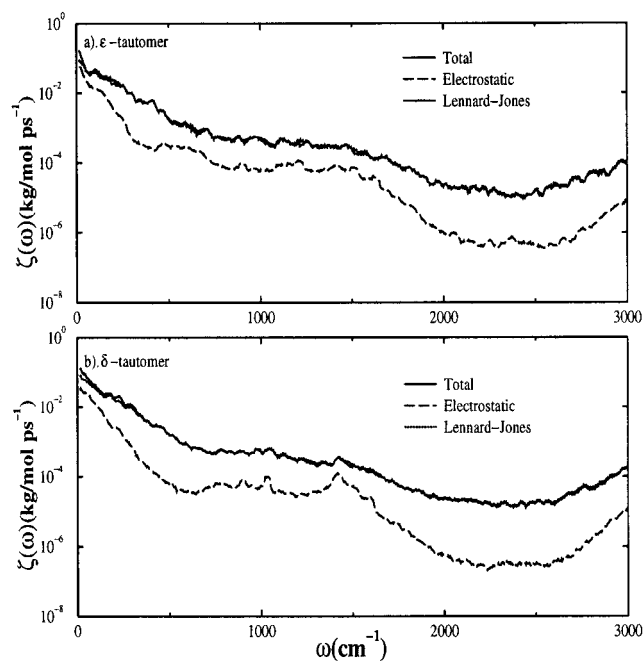
FIGURE 8   The decomposition of the friction spectra for the (a) ϵ- and (b) δ-tautomers into Coulombic and Lennard–Jones contributions. Also shown for comparison are the total spectra. The data were smoothed for visual clarity.

tuating force autocorrelation function were performed for the ϵ-tautomer. The first involved separating the correlation function according to segments of the system. In one such decomposition the system was divided into three segments—the protein, the heme, and the solvent. From Fig. 9 a, it is obvious that the self terms of the protein, heme, and solvent very closely reproduce the total friction spectrum. Any cooperative interactions between these groups is negligible.

A second decomposition based on individual residues was performed to investigate the applicability of the IBC model. Cross correlations, although contributing to the friction kernel, have little influence on the friction spectrum in the vicinity of the CO vibrational frequency. Fig. 10, a and b, demonstrates this fact. This indicates that the relaxation of the CO molecule takes place via a series of successive, uncorrelated collisions with residues in the myoglobin pocket.

The pocket residues

The residues that line the myoglobin pocket are Leu[29], Leu[32], Phe[43], Val[68], His[64], and Ile[107]. Because these residues act as nearest neighbors to the CO molecule, their respective contributions to the friction spectrum were assessed. The resulting spectra are pictured in Fig. 11 a–f. It is clear from Fig. 11 that the tautomeric state of the distal histidine does not affect the friction exerted by Phe[43] and Ile[107] on the CO molecule. Although the average distances of the CO molecule from Phe[43] in each of the tautomers are

FIGURE 7   The 300 K distribution of the fluctuating force felt along the CO bond for the ϵ- and δ-tautomers as labeled in the figure.
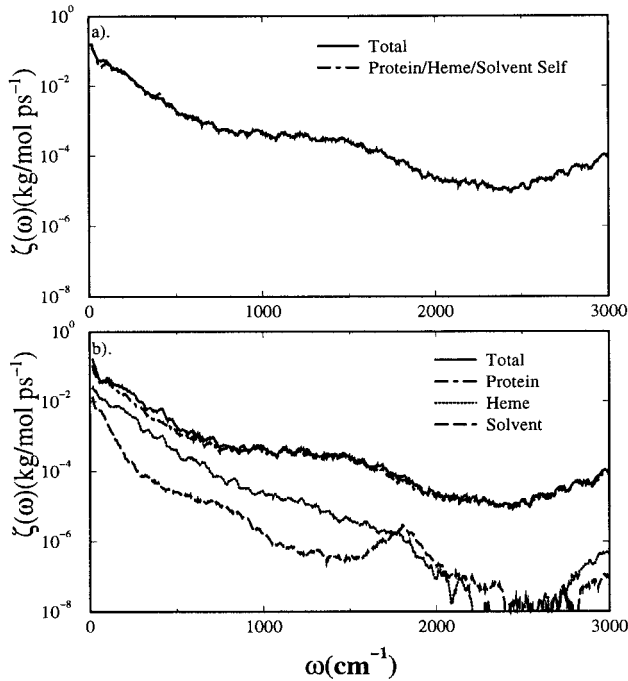
FIGURE 9   A look at the protein, heme, and solvent contributions on the total friction spectrum of the CO bond at 300 K for the ϵ-tautomer. (*a*) The total spectrum and the spectrum obtained by decomposing the force autocorrelation. (*b*) The friction spectra of each of the components as labeled in the figure. All spectra have been smoothed for visual clarity.
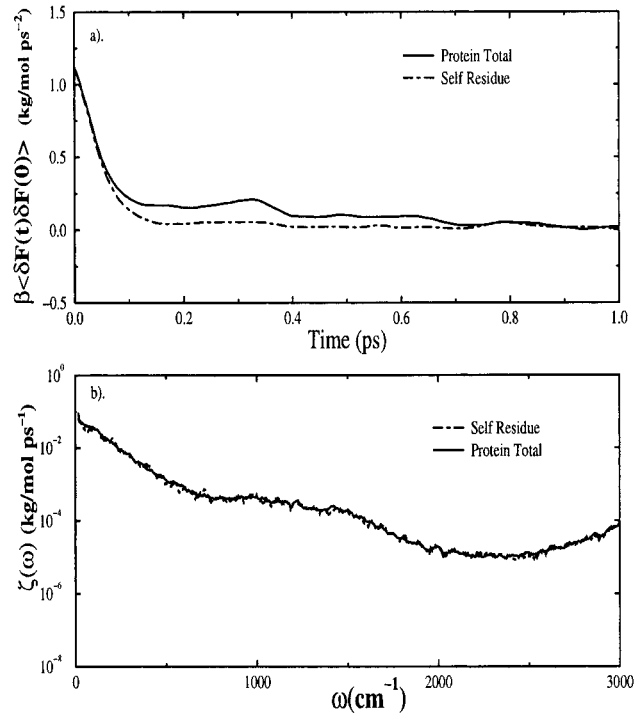
FIGURE 10   (*a*) The fluctuating force autocorrelation function of the protein on the CO bond and the friction kernel calculated from the self terms with respect to the individual residues calculated at 300 K for the ϵ-tautomer. (*b*) The corresponding friction spectra. The spectra have been smoothed for visual clarity.

comparable, this is not so for Ile[107]. The CO tends to be considerably further from Ile[107] in the ϵ-tautomer pocket than in the δ-tautomer pocket. Residues Leu[29], Val[68], and the heme contribute more to CO relaxation in the δ-tautomer than they do in the ϵ-tautomer.

The dominant contribution to the relaxation for each of these components results from van der Waals contacts. The drop in the heme friction spectrum for the ϵ-tautomer shown in Fig. 11 *f* is also due to a subsequent drop in the van der Waals fluctuations, as well as the electrostatic contributions. This is interesting because, on the average, the CO molecule is closer to the heme in the ϵ-tautomer (see Table 4).

The observed distance dependence could be due to different locations of the CO molecule in the pocket or a change in pocket geometry resulting from the tautomeric state. We found that the average distance between the center of mass of Ile[107] and the heme was $\sim$10.3 Å for both tautomers. The distance between the N_ϵ and the Ile[107] center-of-mass was found to be $\sim$1.5 Å closer in the δ-tautomer pocket than in the ϵ-tautomer pocket. The average distances within the pocket indicate that the CO molecule in the ϵ-tautomer has more room in which to move about. To confirm this possibility, the coefficient of diffusion D of the center-of-mass of the CO molecule was calculated. This was done noting that, at intermediate times,

$$\langle |\mathbf{R}(t) - \mathbf{R}(0)|^2 \rangle \rightarrow 6Dt, \qquad (25)$$

where D is the diffusion coefficient, $\mathbf{R}(t)$ is the position of the center-of-mass of the CO molecule at time t. In the limit

of hard sphere collisions, the mean collision frequency α can be extracted easily from the diffusion coefficient of the Enskog model via

$$\alpha = \frac{1}{D\beta m}, \qquad (26)$$

where $\beta = 1/k_b T$ and m is the mass of the oscillator. Using Eq. 25, diffusion coefficients of 4.53×10^{-6} cm^2/s and 1.43×10^{-6} cm^2/s were calculated for the ϵ and δ-tautomer, respectively. This translates to mean collision frequencies of 200 and 635 ps^{-1}. These values indicate that the CO molecule in the δ-pocket does experience more translational restraint and undergoes more collisions per unit time than the CO in the ϵ-tautomer pocket. This extra mobility of the CO molecule in the ϵ-tautomer pocket may be a cause of the drop in the heme contribution to the friction as is addressed in the Appendix.

The role of the distal histidine 64

The direct effect of the distal histidine on CO dynamics and relaxation was examined. Table 5 lists the average distances of the carbon and oxygen of the CO molecule from the N_ϵ and, if applicable, the corresponding H_ϵ. The CO molecule is considerably closer to N_ϵ in the δ-tautomer, with the oxygen atom being closer than the carbon atom. Naively, we might find that this is in accord with a simple point
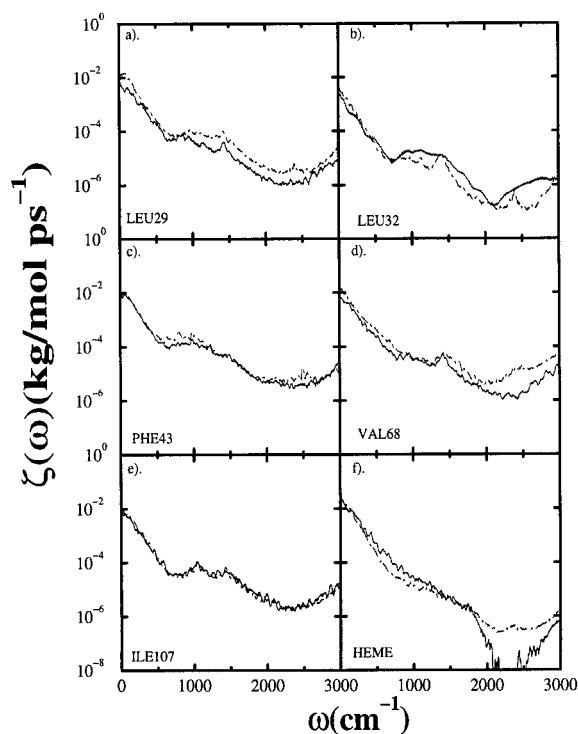
FIGURE 11 The individual components of the friction spectrum due to (a) Leu[29], (b) Leu[32], (c) Phe[43], (d) Val[68], (e) Ile[107], and (f) the heme. The solid and dashed lines represent the ϵ- and δ-tautomers, respectively. The simulations were carried out at 300 K and the data were smoothed for visual clarity.

TABLE 5 The average distance of the carbon and oxygen atoms of the CO molecule from the N_ϵ and H_ϵ of the distal histidine, His[64], at 300 K

	R_C^ϵ	R_O^ϵ	R_C^δ	R_O^δ
N_ϵ	4.46	4.72	3.73	3.60
H_ϵ	4.08	4.35		

The superscript denotes the tautomer. The distances are in Å.

nents differ considerably -0.075 versus 0.392 kcal/(mol Å). This seems to imply that cross correlations are significant because the overall zero-time fluctuation for the δ-tautomer is higher. The Coulombic and Lennard–Jones fluctuations are positively correlated in the δ-tautomer, but are actually anticorrelated in the ϵ-tautomer counterpart. The origin of this effect stems from the CO interaction with the N_ϵ of the histidine.

In the ϵ-tautomer, the carbon and oxygen atoms each feel a strong electrostatic attraction to the H_ϵ. The CO tends to align itself with either its carbon or oxygen atom pointing toward the nitrogen. This is demonstrated in Fig. 13 a, in which the N_ϵ CO angle is plotted as a function of time, indicating that there is a barrier to rotation. This flipping behavior is reminiscent of the proposed two-state orientational behavior of CO in its photolyzed state (Ma et al., 1997; Meller and Elber, 1998).

The orientation of the CO in the δ-tautomer pocket is quite different. The CO molecule moves toward the N_ϵ and avoids the repulsion it feels in the ϵ-tautomer by straddling

charge model fit to the experimental dipole moment showing the oxygen to be the positive pole of the CO molecule. However, ab initio quantum chemical calculations have demonstrated that it is the midbond of the CO molecule that is most strongly attracted to the imidazole's N_ϵ in the gas phase, in which the minimum distance was found to be 3.46 Å (Straub and Karplus, 1991).

In Fig. 12, the histidine components of the force correlation functions for both tautomers are presented. As expected, the zero-time fluctuation for the δ-tautomer is larger than for the ϵ-tautomer. As is shown in Fig. 12 b and c, the fluctuations of the pure electrostatic components are similar -0.413 versus 0.375 kcal/(mol Å) for the δ- and ϵ-tautomers, respectively. However, the Lennard–Jones compo-

TABLE 4 The average distance of the carbon and oxygen atoms and the center of mass of the CO molecule from select residues in the myoglobin pocket

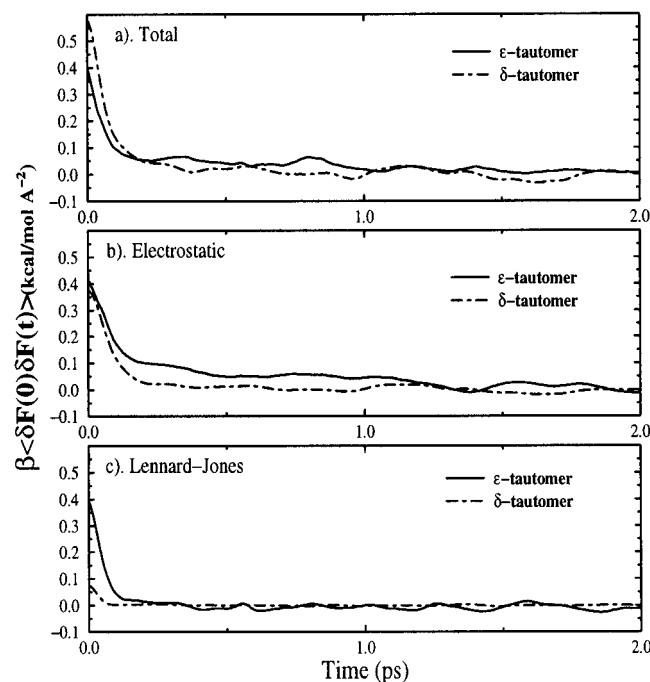|	C		O		COM	
Residue	ϵ	δ	ϵ	δ	ϵ	δ
Leu[29]	6.12	5.68	6.14	5.94	6.11	5.81
Phe[43]	7.15	7.40	7.23	7.25	7.19	7.31
Val[68]	6.71	6.37	6.78	6.38	6.73	6.36
Ile[107]	8.48	6.60	8.31	6.77	8.37	6.69
Heme	4.59	5.39	4.69	5.13	4.62	5.22

The distances are in Å.

FIGURE 12 (a) The friction kernel contributions of the distal histidine in its two tautomeric states. (b) The electrostatic component of the friction kernel due to the distal histidine in its two tautomeric states. (c) The Lennard–Jones component of the friction kernel due to the distal histidine in its two tautomeric states.
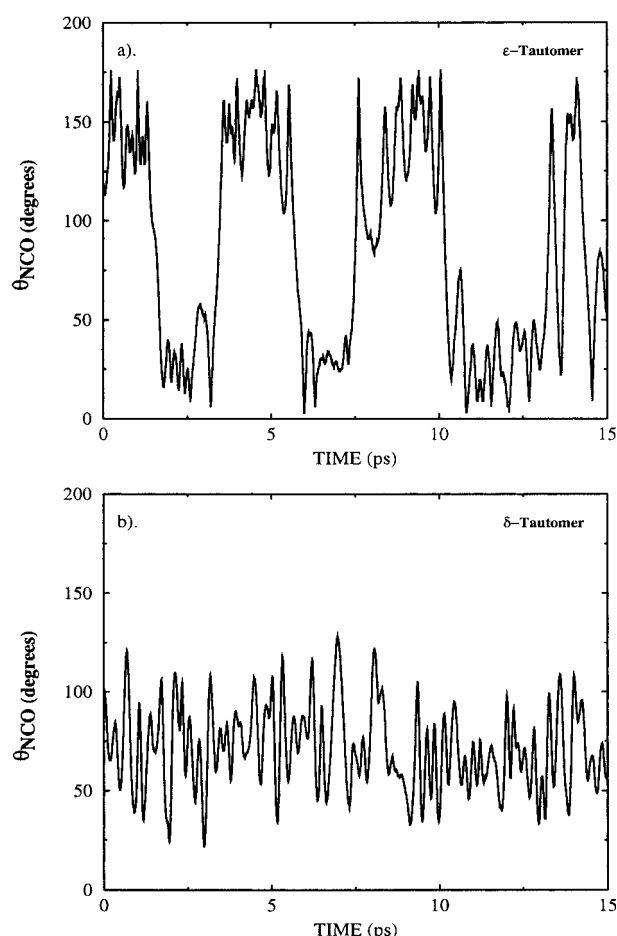
FIGURE 13　The angle formed by N_ϵ, C, and O atoms as a function of time for the (a) ϵ- and (b) δ-tautomers at 300 K.

the unprotonated N_ϵ. The N_ϵ CO angle as a function of time is plotted in Fig. 13 b. In the δ-tautomer, the N_ϵ CO angle tends to fluctuate around a single minimum, and there is no apparent flipping or realignment of the CO dipole with respect to the histidine nitrogen.

The fluctuating force felt by the ϵ-tautomer histidine along the CO bond is a combination of Coulombic and van der Waals forces. Although the average CO–N_ϵ distance is greater with the ϵ-tautomer, the distance of closest approach is smaller than in the δ-tautomer.

In the ϵ-tautomer, the electrostatic force pulls the molecule in as the van der Waals force pushes it away. This results in an anticorrelation between the two force components. In the δ-tautomer, the force is dominated by electrostatic fluctuations with a weaker Lennard–Jones repulsion. As a result, there is not as high a degree of anticorrelation as is seen with the ϵ-tautomer. In fact, the forces are slightly positively correlated. The difference in the cross correlations between the two tautomers manifests itself in the low frequency range of the friction spectrum and contributes little to the spectrum in the high frequency range of the CO molecule.

Have all of the key residues been included in our discussion? Shown in Fig. 14 are the total friction spectrum of the CO in the ϵ-tautomer pocket and the self spectrum of the residues listed in Table 4. The match is quite satisfactory in the frequency range of the CO molecule indicating the dominant influence of what we have identified as the key residues.

SUMMARY AND CONCLUSIONS

This work has investigated several aspects of vibrational relaxation of carbon monoxide in myoglobin. The data suggest that a harmonic treatment of the surrounding protein and solvent is a reasonable approximation that results in accurate values of vibrational relaxation times. The calculated vibrational relaxation times presented above suggest that the distal histidine of carbonmonoxy myoglobin is in the ϵ-tautomeric state. This observation is consistent with recent resonance Raman studies of D_2O effects on the vibrational frequency shifts of bound CO (Unno et al., 1998). In addition, a detailed analysis designed to pinpoint key residues in the relaxation process in myoglobin has been presented. The residues are those that form the inner wall of the myoglobin pocket—Leu[29], Leu[33], Phe[43], His[64], Val[68], Ile[107], and the heme. In our simulations, the relaxation was dominated by short-ranged van der Waals interactions with these residues. The data presented here suggest that the mechanism of vibrational relaxation of CO in myoglobin takes places through successive, noncorrelated collisions with the pocket residues. This supports the validity of an IBC model for modeling the relaxation of the CO vibration.

APPENDIX A

When dealing with problems in which electrostatic interactions are essential, it is wise to investigate the effect of the method used in treating the long-range interactions. The method used in this study involved a simple
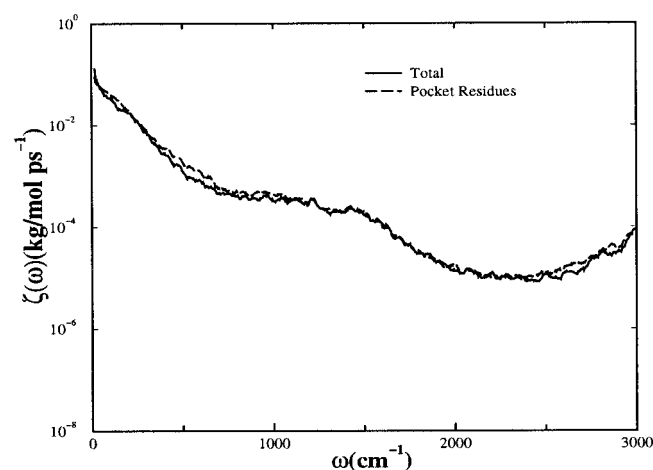

FIGURE 14　Comparison of the total friction spectrum and that obtained using only the residues listed in Table 4 for the ϵ-tautomer at 300 K.

FIGURE A1 The electrostatic components to the friction spectrum of the ϵ-tautomer as a function of radius from the CO center of mass as listed in the figure. The dynamics of the CO molecule from which the forces were collected was run using a spherically truncated potential switched off from 9.5 to 10.5 Å.
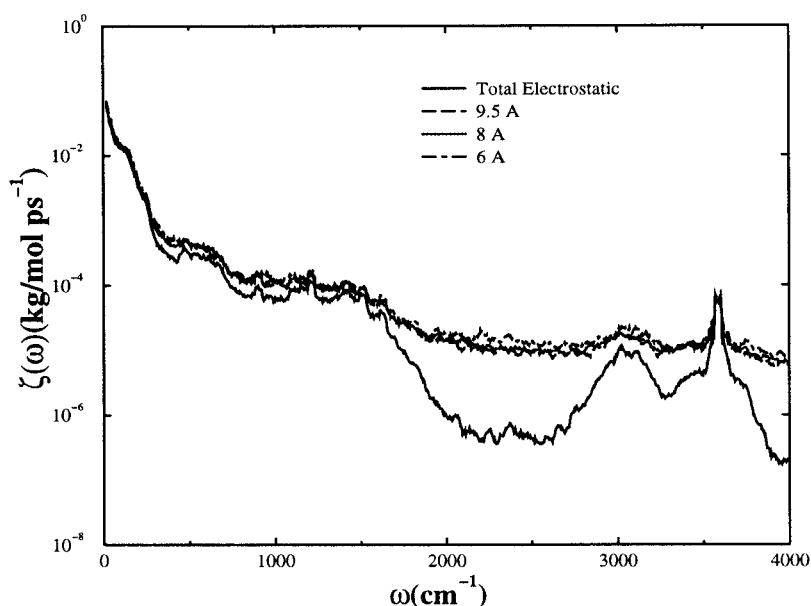
potential truncation in which the potential was tapered to zero using a switching function from 9.5 to 10.5 Å. Fig. A1 displays the electrostatic friction spectra in the vicinity of the CO oscillator frequency calculated for atoms lying within varying radii. Keep in mind that the dynamics from which the forces were calculated used the cutoff mentioned above. Therefore, the forces felt along the CO bond at radii less than the cutoff do not fall to zero gradually. The data in the figure depict a relatively large increase in the electrostatic contribution at radii less than or equal to 9.5 Å, which is the beginning of the potential cutoff. Several additional simulations were run to check the possibility that the potential cutoff used was not large enough. The same trend was seen in simulations in which the potential function was switched from 11.0 to 12.0 Å and when the switching function spanned over 4.0 Å instead of 1.0 Å. In each instance, the electrostatic force spectrum was lower at high frequency when including all atoms within the potential cutoff than when using a subset of those atoms within some radius.

The switching function acts to screen the CO from long-range interactions. Which interactions are most affected by this screening? Fig. A2 displays the total friction spectrum for the ϵ-tautomer for each of the radii specified. Although there is some change in the friction spectrum, it is

minimal. In Fig. A2, the changes in the friction spectrum for the protein, heme, and solvent are pictured. The protein shows little effect as the radii decrease, whereas the heme and solvent show the most significant effects. This is somewhat surprising because of the relatively nonpolar nature of the CO molecule. The heme has two polar groups pointing away from the pocket and toward the solvent. These groups tend to be between 9 to 11 Å away from the CO molecule. As the cutoff radius is decreased, the influence of these groups is attenuated. The same can be said of the solvent molecules. This suggests that the anisotropy of the system is the difficulty. Although the protein itself is more or less spherically symmetric about the pocket, this is not the case where the heme and solvent molecules are concerned.

One more check into this phenomenon is to alter the charge distribution of the CO molecule. Three 15-ps simulations of the ϵ-tautomer were run under the conditions described above with the charges on the carbon and oxygen set to $+0.021e$ and $-0.021e$, respectively, to fit the experimentally measured electric dipole moment. The same behavior is noted with regards to the electrostatic spectrum. However, as the overall electrostatic contribution is much smaller, there is no observed change in the total spectrum. Clearly, using these charges, a nearest neighbor collision model would

FIGURE A2 The electrostatic components of the friction spectrum of the ϵ-tautomer due to the protein as a function of radius from the CO center of mass as listed in the figure. The dynamics of the CO molecule from which the forces were collected was run using a spherically truncated potential switched off from 9.5 to 10.5 Å.
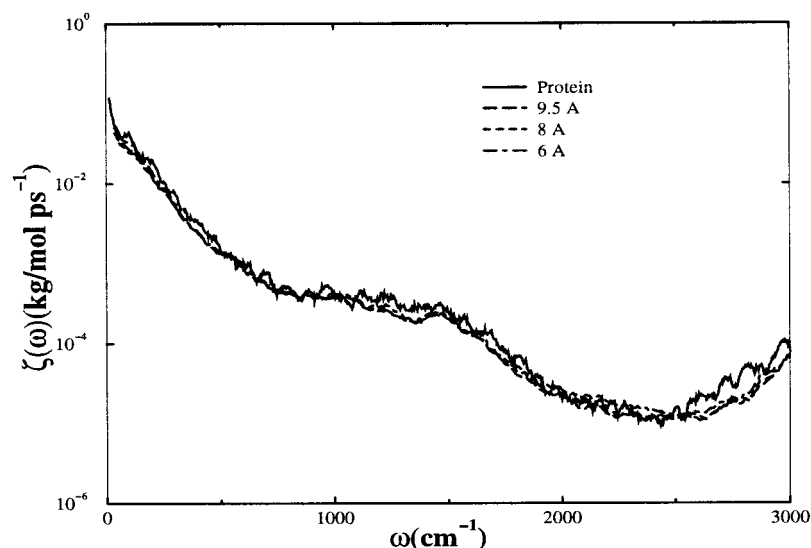
accurately describe the mechanism of CO vibrational relaxation. The resulting T_1 time calculated using these charges is ~ 1.0 ns. This value is approximately 1.5 times as large as that calculated using the three site model indicating a small but nonetheless nonzero dependence on the charges used. This decrease in relaxation rate stems not only from the decrease in the electrostatic contributions but also a decrease in the Lennard–Jones contributions, pointing once again to the intricate nature of interactions in this system. The fluctuating force distribution functions, however, showed little qualitative change, and it is believed that, based on other studies (Sagnella and Tuckerman, 1998; Meller and Elber, 1998), the use of the Ewald method would not affect the conclusions drawn from the distributions presented in this work.

Because the CO dynamics evolved using the potential function and cutoff described in Computational Model and Methods, the complete force from the simulation was used in calculating the results presented here. Although our results show a change in the time-dependent friction spectrum as a function of the electrostatic potential cutoff, the mechanism of energy relaxation is dominated by short-range forces and binary collisions. This implies that we are unlikely to see a large difference in T_1 for other choices of electrostatic potential truncation.

APPENDIX B: DERIVATION OF T_1 ERROR ESTIMATE

Let x be a function of several variables so that

$$x = f(a, b, \ldots). \quad (B1)$$

Consequently, any infinitesimal change in x is

$$\delta x = \frac{\partial f}{\partial a}\,\delta a + \frac{\partial f}{\partial b}\,\delta b + \cdots. \quad (B2)$$

Squaring this gives

$$(\delta x)^2 = \left(\frac{\partial f}{\partial a}\,\delta a + \frac{\partial f}{\partial b}\,\delta b + \cdots\right)^2. \quad (B3)$$

If the fluctuations in the set of variables $\{a, b, \ldots\}$ are indeed the result of random uncertainties, the sum of the cross terms will be zero and

$$\delta x^2 = \left(\frac{\partial f}{\partial a}\,\delta a\right)^2 + \left(\frac{\partial f}{\partial b}\,\delta b\right)^2 + (\cdots)^2. \quad (B4)$$

Summing over all data points N and then dividing by N we find

$$\sum_{i=1}^{N} \frac{\delta x_i^2}{N} = \left(\frac{\partial f}{\partial a}\right)^2 \sum_{i=1}^{N} \frac{\delta a_i^2}{N} + \left(\frac{\partial f}{\partial b}\right)^2 \sum_{i=1}^{N} \frac{\delta b_i^2}{N} + (\cdots). \quad (B5)$$

If the infinitesimal change in x is about the mean, $\delta x_i = x_i - \bar{x}$, and the term on the left hand side of the above equation is simply the square of the standard deviation of $x(\sigma_x)$. Therefore,

$$\sigma_x^2 = \left(\frac{\partial f}{\partial a}\right)^2 \sigma_a^2 + \left(\frac{\partial f}{\partial b}\right)^2 \sigma_b^2 + (\cdots)^2. \quad (B6)$$

In terms of the vibrational relaxation time, in which $T_1 = \mu/\bar{\zeta}$, we have

$$\mu \frac{\partial f}{\partial \bar{\zeta}} = -\frac{\mu}{\bar{\zeta}^2} \quad (B7)$$

and

$$\sigma_{T_1}^2 = \left(\frac{\mu}{\bar{\zeta}^2}\right)^2 \sigma_\zeta^2, \quad (B8)$$

which leads to the expression in Eq. 22

$$\sigma_{T_1} = \mu \frac{\sigma_\zeta}{\bar{\zeta}^2}. \quad (B9)$$

REFERENCES

Bader, J. S., and B. J. Berne. 1994. Quantum and classical relaxation rates from classical simulations. *J. Chem. Phys.* 100:8359–8366.

Berne, B. J., M. E. Tuckerman, J. E. Straub, and A. L. R. Bug. 1990. Dynamic friction on rigid and flexible bonds. *J. Chem. Phys.* 93:5084–5095.

Brooks, B. R., R. D. Bruccoleri, B. O. Olafson, D. J. States, S. Swaminathan, and M. Karplus. 1983. CHARMM: a program for macromolecular energy minimization and dynamics calculations. *J. Comp. Chem.* 4:187–217.

Cheng, X., and B. P. Schoenborn. 1991. Neutron diffraction study of carbon-monoxymyoglobin. *J. Mol. Biol.* 220:381–399.

Cho, M., G. R. Fleming, S. Saito, I. Ohmine, and R. M. Stratt. 1994. Instantaneous normal mode analysis of liquid water. *J. Chem. Phys.* 100:6672–6683.

Gnanakaran, S., and R. M. Hochstrasser. 1996. Vibrational relaxation of HgI in ethanol: equilibrium molecular dynamics simulations. *J. Phys. Chem.* 105:3486–3496.

Goodyear, G., and R. M. Stratt. 1996. The short time intramolecular dynamics of solutes in liquids. I. An instantaneous normal mode theory for friction. *J. Chem. Phys.* 105:10050–10071.

Goodyear, G., and R. M. Stratt. 1997. The short time intramolecular dynamics of solutes in liquids. II. Vibrational population relaxation. *J. Chem. Phys.* 107:3098–3120.

Hanson, J. C., and B. P. Schoenborn. 1981. Real space refinement of neutron diffraction data from sperm whale myoglobin. *J. Mol. Biol.* 153:117–146.

Harris, C. B., D. E. Smith, and D. Russell. 1990. Vibrational relaxation of diatomic molecules in liquids. *Chem. Rev.* 90:481–488.

Hill, J. R., D. D. Dlott, M. D. Fayer, K. A. Peterson, C. W. Rella, M. M. Rosenblatt, K. S. Suslick, and C. J. Ziegler. 1995. Vibrational dynamics of carbon monoxide in model heme compounds. 6-coordinated metalloporphyrins (M = Fe, Ru, Os). *Chem. Phys. Lett.* 244:218–223.

Hill, J. R., D. D. Dlott, C. W. Rella, K. A. Peterson, S. M. Decatur, S. G. Boxer, and M. D. Fayer. 1996a. Vibrational dynamics of carbon monoxide at the active sites of mutant heme proteins. *J. Phys. Chem.* 100:12100–12107.

Hill, J. R., A. Tokmakoff, K. A. Peterson, B. Sauter, D. Zimdars, D. D. Dlott, and M. D. Fayer. 1994. Vibrational dynamics of carbon monoxide at the active sites of myoglobin: picosecond infrared free-electron laser pump-probe experiments. *J. Phys. Chem.* 98:11213–11219.

Hill, J. R., C. J. Ziegler, K. S. Suslick, D. D. Dlott, C. W. Rella, and M. D. Fayer. 1996b. Tuning the vibrational relaxation of CO bound to heme and metalloporphyrin complexes. *J. Phys. Chem.* 100:18023–18032.

Huffaker, J. N. 1976. Diatomic molecules as perturbed Morse oscillators. I. Energy levels. *J. Chem. Phys.* 64:3175–3181.

Jorgensen, W. L., J. Chandrasekhar, J. D. Madura, R. W. Impey, and M. L. Klein. 1983. Comparison of simple potential functions for simulations of liquid water. *J. Chem. Phys.* 79:926–935.

King, J. C., J. Z. Zhang, B. J. Schwartz, and C. B. Harris. 1993. Vibrational relaxation of $M(CO)_6$ (M = Cr, Mo, W): effect of metal mass on vibrational cooling dynamics and non-Boltzmann internal energy distributions. *J. Chem. Phys.* 99:7595–7601.

Landanyi, B., and R. M. Stratt. 1998. The short-time dynamics of vibrational relaxation in molecular fluids. *J. Phys. Chem. A.* 102:1068–1082.

Lim, M., T. A. Jackson, and P. A. Anfinrud. 1995. Mid-infrared vibrational spectrum of CO after photodissociation from heme: Evidence for a ligand docking site in the heme pocket of hemoglobin and myoglobin. *J. Chem. Phys.* 102:4355–4366.

Litovitz, T. A. 1957. Theory of ultrasonic thermal relaxation times in liquids. *J. Chem. Phys.* 26:469–473.

Ma, J., S. Huo, and J. E. Straub. 1997. Molecular dynamics simulation study of the B-states of solvated carbon monoxymyoglobin. *J. Am. Chem. Soc.* 119:2541–2551.

MacKerell, A. D., Jr., D. Bashford, M. Bellott, R. L. Dunbrack, Jr., M. J. Field, S. Fischer, J. Gao, H. Guo, S. Ha, D. Joseph, L. Kuchnir, K. Kuczera, F. Lau, C. Mattos, S. Michnick, T. Ngo, D. T. Nguyen, B. Prodhom, B. Roux, M. Schlenkrich, J. C. Smith, R. Stote, J. Straub, J. Wiorkiewicz-Kuczera, and M. Karplus. 1992. Self-consistent parameterization of biomolecules for molecular modeling and condensed phase simulations. *FASEB J.* 6:A143.

Madan, B., and T. Keyes. 1993. Unstable modes in liquids density of states, potential energy and heat capacity. *J. Chem. Phys.* 98:3342–3350.

Madan, B., T. Keyes, and G. Seeley. 1990. Diffusion in supercooled liquids via normal mode analysis. *J. Chem. Phys.* 92:7565–7569.

Meller, J., and R. Elber. 1998. Computer simulations of carbon monoxide photodissociation in myoglobin: structural interpretation of the B-states. *Biophys. J.* 74:789–802.

Owrutsky, J. C., M. Li, B. Locke, and R. M. Hochstrasser. 1995. Vibrational relaxation of the CO stretch vibration in hemoglobin-CO, myoglobin-CO and protoheme-CO. *J. Phys. Chem.* 99:4842–4846.

Oxtoby, D. W. 1979. Hydrodynamic theory for vibrational dephasing in liquids. *J. Chem. Phys.* 70:2605–2610.

Oxtoby, D. W. 1981. Vibrational population relaxation in liquids. *Adv. Chem. Phys.* 47:487–519.

Press, W. H., B. P. Flannery, S. A. Tuekolsky, and W. T. Vetterling. 1989. Numerical Recipes: The Art of Scientific Computing. chap. 12. Cambridge University Press, New York, 381–397.

Sagnella, D. E., and M. E. Tuckerman. 1998. An empirical valence bond model for proton transfer in water. *J. Chem. Phys.* 108:2073–2083.

Schlichting, I., J. Berendzen, G. N. Phillips, Jr., and R. M. Sweet. 1994. Crystal structure of photolysed carbonmonoxy-myoglobin. *Nature.* 371:808–812.

Seeley, G., and T. Keyes. 1989. Normal-mode analysis of liquid-state dynamics. *J. Chem. Phys.* 91:5581–5586.

Seeley, G., T. Keyes, and B. Madan. 1991. Isobaric diffusion constants in simple liquids and normal mode analysis. *J. Chem. Phys.* 95:3847–3849.

Straub, J. E., and M. Karplus. 1991. Molecular dynamics study of the photodissociation of carbon monoxide: ligand dynamics in the first 10 ps. *Chem. Phys.* 158:221–248.

Unno, M., J. F. Christian, J. S. Olson, T. Sage, and P. M. Champion. 1998. Evidence for hydrogen bonding effects in the iron ligand vibrations pf carbonmonoxy myoglobin. *J. Am. Chem. Soc.* 120:2670–2671.

Wan, Y., and R. M. Stratt. 1994. Liquid theory for the instantaneous normal modes of a liquid. *J. Chem. Phys.* 100:5123–5138.

Whitnell, R. M., K. R. Wilson, and J. T. Hynes. 1992. Vibrational relaxation of a dipolar molecule in water. *J. Chem. Phys.* 96:5354–5369.

Whitnell, R. M., K. R. Wilson, and J. T. Hynes. 1990. Fast vibrational relaxation for a dipolar molecule in a polar solvent. *J. Phys. Chem.* 94:8625–8628.

Wu, T. M., and R. F. Loring. 1992. Phonons in liquids: a random walk approach. *J. Chem. Phys.* 97:8568–8575.

Zwanzig, R. 1961. Theory of vibrational relaxation in liquids. *J. Chem. Phys.* 34:1931–1935.

Zwanzig, R. 1973. Nonlinear generalized Langevin equation. *J. Stat. Phys.* 9:215–220.